Frontiers in Bioscience Landmark

Front. Biosci. (Landmark Ed) **2024**; 29(1): 39
https://doi.org/10.31083/j.fbl2901039

Original Research

Bioinformatics Analysis Identifies *PLA2G7* as a Key Antigen-Presenting Prognostic Related Gene Promoting Hepatocellular Carcinoma through the STAT1/PD-L1 Axis

Sihang Guo[1], Qinhe Yang[1,*]

[1]School of Traditional Chinese Medicine, Jinan University, 510632 Guangzhou, Guangdong, China
*Correspondence: tyangqh@jnu.edu.cn (Qinhe Yang)
Academic Editor: Fu Wang
Submitted: 26 July 2023 Revised: 1 December 2023 Accepted: 18 December 2023 Published: 23 January 2024

Abstract

Background: Antigen presentation may be an important factor contributing to immune evasion in cancer. This study investigated antigen-presenting prognostic related genes (APPGs) and their potential mechanisms in hepatocellular carcinoma (HCC). **Methods**: We constructed a score built upon the core APPGs (APP.Score) through nonnegative matrix factorization (NMF) clustering, weighted gene co-expression network analysis (WGCNA), random forest (RF), and least absolute shrinkage and selection operator (LASSO) methods. We also compared the clinical and molecular characteristics of different APP.Score. Furthermore, *in vitro* experiments were conducted to validate the expression of core APPGs and investigate the effects of phospholipase A2, group 7 (PLA2G7) knockdown on HCC cell development and programmed death-ligand 1 (PD-L1) expression. **Results**: APP.Score was positively correlated with immune cell infiltration and levels of immune checkpoint inhibitor-related genes, and negatively correlated with overall survival (OS). The area under the curve values were 0.734, 0.747, and 0.679 for survival periods of 1, 2, and 3 years, respectively, indicating that APP.Score could be an independent prognostic factor for patients with HCC. OS of the high expression group of these genes, including *PLA2G7*, musculin, heat shock protein family A, secreted phosphoprotein 1, and neutrophil cytosolic factor 2 (*NCF2*) was lower than that of their low expression group. Moreover, the upregulation of key components of APPGs, except *NCF2*, was observed in HCC. The inhibition of PLA2G7 suppressed HCC progression and reduced PD-L1 and phosphorylated signal transducer and activator of transcription 1 (p-STAT1)/STAT1 levels in HepG2 and Huh-7 cells. Remarkably, the decrease in PD-L1 expression caused by PLA2G7 silencing was reversed upon treatment with a STAT1 activator. **Conclusion**: The results of this study show that APP.Score could be an independent prognostic factor for patients with HCC, and that PLA2G7 silencing inhibits cancer cell development and PD-L1 expression. We provide a new perspective and potential target for immune research on antigen presentation in HCC.

Keywords: liver cancer; antigen presentation; antigen-presenting prognostic related genes; PLA2G7; APP.Score

1. Introduction

Hepatocellular carcinoma (HCC) is a lethal malignancy globally with a low survival rate [1,2]. It has been estimated that the incidence of HCC has tripled in the last 30 years [3], and the incidence and mortality rates continue to increase [4]. Chemotherapy and immunotherapy are currently the best treatment options for HCC patients [1]. Although preclinical and clinical studies have shown that immune checkpoint inhibitor (ICI) therapy provides survival benefits to a larger population of HCC patients, including those with cholangiocarcinoma [5], most cancer patients still exhibit resistance to ICI blockade [6]. The molecular mechanisms underlying the immune response and evasion in HCC are not fully understood and thus need to be further researched.

There are many predictive biomarkers of immunotherapy in HCC patients, such as tumor mutation burden, the tumor microenvironment (TME), and T cell inflammation. However, these markers have limitations that hinder their clinical application [7–9]. Antigen presentation is essential for triggering the T cell immune response, serving as a link between nonspecific and specific immunity [10]. Antigen-presenting cells (APCs), such as dendritic cells (DCs) and macrophages (MACs), present peptides on major histocompatibility complex class I or II (MHC-I or MHC-II) to naive T cells ($CD8^+$ or $CD4^+$) to activate the immune response [11]. The human MHC is usually referred to as human leukocyte antigen (HLA) [12]. Tumor antigens allow tumor cells to be recognized and killed by $CD8^+$ T cells through the antigen-presenting mechanism [13]. Tumors use various escape mechanisms in AP to evade immune recognition, ultimately leading to tumor immune escape [14]. However, we did not find any relevant studies on how antigen-presenting prognostic (APP) related genes (APPGs) of HCC affect the therapeutic immune response and whether they can predict the prognosis.

Currently, bioinformatics analyses such as nonnegative matrix factorization (NMF) clustering, weighted gene co-expression network analysis (WGCNA), random forest (RF) models, and least absolute shrinkage and selection operator (LASSO) have been widely applied to data min-

ing, genomics, proteomics, and other research fields related to disease [15–18]. NMF clustering, a matrix decomposition method, has been widely used in prognosis-related gene studies of various cancers [15,19]. For example, Gao *et al*. [16] utilized NMF clustering to analyze m6A RNA methylation regulators, revealing that the methylation-mediated TME regulates intercellular communication in tumor growth and antitumor immune regulation processes. WGCNA can describe the interaction between genes by constructing a gene co-expression network. For instance, Tian *et al*. [17] identified core modules and central genes associated with breast cancer using WGCNA. RF, an ensemble learning algorithm, can be used to screen prognostic markers for various cancers such as prostate, breast, and lung cancers [20–22]. LASSO is a linear regression model and bioinformatics algorithm commonly used for data analyses in cancer. For example, Kang *et al*. [23] used a LASSO model combined with other indicators to predict lymph node metastasis in patients with T1 rectal cancer.

Here, we screened the APPGs of HCC using public datasets and bioinformatics analysis to predict the prognosis of patients with HCC. Furthermore, we conducted preliminary *in vitro* experiments to explore the impact of key APPGs on HCC cells. Our study lays the foundation for HCC diagnosis and immunotherapy.

2. Materials and Methods

2.1 Research Data Gathering

The Cancer Genome Atlas Liver Hepatocellular Carcinoma (TCGA-LIHC) and Gene set enrichment 14520 (GSE14520) datasets were obtained from TCGA (https://tcga-data.nci.nih.gov/tcga/) and Gene Expression Omnibus (GEO, https://www.ncbi.nlm.nih.gov/geo/) datasets. APPGs were obtained through ImmPort (https://www.immport.org/home).

Construction of a Prognostic Model for Scores Built upon the Core APPGs

Based on the TCGA-LIHC dataset, prognosis-related APPGs were obtained by univariate Cox analysis ($p < 0.01$). Based on these genes, APP-related genotyping (APP. cluster 1 and APP. cluster 2) was obtained by performing NMF clustering and subjected to survival analysis. The expression of all APPGs was analyzed. For the TCGA-LIHC dataset, WGCNA was performed according to AP-related genotyping. The module that was most relevant to APP-related genotyping was found by screening. Genes in the modules were subjected to univariate Cox analysis ($p < 0.01$). Then nine genes were obtained by performing RF analysis (relative importance >0.3). The LASSO model was constructed to obtain the core APPGs, including *KLRB1*, neutrophil cytosolic factor 2 (*NCF2*), *PLA2G7*, msculin (*MSC*), *HSPA6*, secreted phosphoprotein 1 (*SPP1*), *FABP5P7*, in LIHC. A score built upon the core APPGs (APP.Score) was obtained by calculating the formula (APP.Score = –2.2047 × *KLRB1* + 0.0197 × *NCF2* + 1.2247 × *PLA2G7* + 0.7626 × *MSC* + 0.78 × *HSPA6* + 0.7743 × *SPP1* + 0.8317 × *FABP5P7*). GSE14520 was used to externally test the prognostic predictive power of the model. The calculated APP.Score was subjected to survival and receiver operator characteristic curve (ROC) analyses. The seven genes, including *KLRB1*, *NCF2*, *PLA2G7*, *MSC*, *HSPA6*, *SPP1*, *FABP5P7*, in LIHC obtained from the final screening were subjected to survival and expression analysis. The LIHC patients were categorized into two groups (high APP.Score and low APP.Score). **Supplementary Fig. 1** illustrates the study design.

2.2 Immune Cells Infiltration and GSE Analysis

The R package limma (version 3.6.1) was utilized to process the processing of gene expression matrix data. With the addition of APP.Score, immune scores and immune cell infiltration were assessed by the ESTIMATE algorithm and TIMER database, respectively [24,25]. In addition, we analyzed the expression of immune cell marker genes with different APP.Scores of LIHC samples using the TIMER database. The Gene Set Variation Analysis (GSVA) package was used for analyzing the Kyoto Encyclopedia of Genes and Genomes (KEGG, https://www.genome.jp/kegg/) pathway via GSVA [26]. Additionally, correlation analyses were conducted among prognostic scoring, gene scoring, and functional enrichment pathways. Subsequently, the ClusterProfiler R package was utilized for performing GSE analysis (GSEA) based on the APP.Score.

2.3 Mutation and Copy Number Variation Analysis

The mutated genes in the high and low APP.Score groups were analyzed using the "maftools" R package [27]. The copy number variation (CNV) landscape and the assessment of copy number gains or losses at amplified or deleted peaks, was evaluated using GISTIC 2.0 analysis (https://gatk.broadinstitute.org) [28].

2.4 Prediction of Drug Sensitivity

The somatic mutations and CNV profiles were collected from the TCGA-LIHC dataset. The drug sensitivity of the high APP.Score and low APP.Score groups was analyzed using the oncoPredict package (version 0.2) [29].

2.5 Cell Treatment

Human normal hepatic stellate cells (LX-2, AW-CNH008; Abiowell Biotechnology Co., Ltd., Changsha, China) and HCC lines, including HepG2 (AW-CCH024; Abiowell) and Huh-7 (AW-CCH089; Abiowell), were cultured in a humidified incubator at 37 °C and 5% CO_2. Phospholipase A2, group 7 (PLA2G7) silencing (si-PLA2G7) and its negative control (si-NC) were transfected into HepG2 and Huh-7 cells using Lipofectamine 2000 (2028090; Invitrogen, Carlsbad, CA, USA) for a duration of 48 h. All cell lines were validated by short tandem repeat profiling and tested negative for mycoplasma.

2.6 Quantitative Real-time Polymerase chain reaction

The six selected genes were validated by quantitative real-time PCR (qRT-PCR) using a fluorescence qRT-PCR instrument (PIKOREAL96, Thermo, Waltham, MA, USA). Primer sequences were designed utilizing primer 5 software, with β-actin serving as an internal mRNA reference and listed in **Supplementary Table 1**. Relative gene expression was analyzed employing the $2^{-\Delta\Delta Ct}$ method.

2.7 Western Blotting

The cells were lysed, centrifuged, and concentrated. Then the proteins were separated by electrophoresis and electrotransferred to a nitrocellulose membrane. The membrane was incubated overnight at 4 ℃ with the following primary antibodies: killer cell lectin like receptor B1 (KLRB1), PLA2G7, musculin (MSC), heat shock protein family A (HSPA6), secreted phosphoprotein 1 (SPP1), neutrophil cytosolic factor 2 (NCF2), programmed death-ligand 1 (PD-L1), phosphoinositide 3-kinase (PI3K), AKT, phosphorylated signal transducer and activator of transcription 1 (p-STAT1), STAT1, phosphorylated nuclear factor kappa B (p-NF-κB), and NF-κB with β-actin as the internal reference. The membrane was incubated with horseradish peroxidase-conjugated goat anti-mouse/rabbit immunoglobulin G (IgG) secondary antibody at 37 ℃ with shaking for 90 min, followed by the development and visualization of the proteins. After washing with phosphate buffer, the membrane was immersed in ECL reaction solution and incubated at room temperature for 1 minute. The protein was exposed and imaged using a chemiluminescence imaging system (ChemiScope 6100, CLINX, Shanghai, China). Detailed antibody information was provided in **Supplementary Table 2**.

2.8 Cell Counting Kit-8 Assay

The Cell Counting Kit-8 (CCK-8) assay was used to measure cell proliferation. Cells were separately cultured for different time points (12, 24, 48 h) and then added to medium containing 10% CCK-8 (NU679, DOJINDO Laboratories, Kumamoto, Japan). The cells were incubated at 37 ℃ for an additional 4 h, and their optical density values were analyzed at 450 nm.

2.9 Colony Formation Assay

The cells were digested into single cells, and 200 cells/per well were seeded and maintained for 10 days. After the cells were fixed in 4% paraformaldehyde and stained with crystalline violet, photographs were taken for observation.

2.10 Wound Healing Assay

As previously described [30], a monolayer of cells was scratched. The cells were rinsed three times with phosphate-buffered saline to remove the scratched cells, and serum-free medium was added. Cell healing was observed under an optical microscope (DSZ2000X, Beijing Zhongyantaihe Medical Instrument Co., Ltd., Beijing, China) at 0 and 48 h.

2.11 Transwell Assay

Matrigel (354262, Becton Dickinson and Co., Franklin, NJ, USA) that had been prediluted was added to the upper chamber, followed by the addition of a cell suspension of 2×10^4 to the same chamber. The lower chamber was filled with medium containing 20% fetal bovine serum. After incubating and wiping down the upper chamber, the cells were fixed, stained, and observed under an optical microscope. The results were analyzed using ImageJ software (version 1.49, National Institutes of Health, Bethesda, MD, USA).

2.12 Flow Cytometry (FCM)

Cell apoptosis was detected using an apoptosis detection kit (KGA1030, KeyGEN BioTECH, Jiangsu, China) through the instructions. After incubation, the results were immediately evaluated using FCM (A00-1-1102, Beckman, Brea, CA, USA).

2.13 Immunofluorescence Staining

Cells were fixed, permeabilized, and closed. Then cells were incubated overnight at 4 °C with primary antibody against PD-L1 (1:50, 28076-1-AP, Proteintech, Chicago, IL, USA), followed by incubation for 90 min at 37 °C with anti-rabbit IgG secondary antibody (1:200, SA00013-4, Proteintech). Finally, the cell nuclei were stained and visualized under a fluorescence microscope (BA210T, Motic Microscopes, Chautauqua County, NY, USA).

2.14 Statistical Evaluation

We conducted our statistical analysis and data visualization by utilizing R version 3.6.1 along with the ggplot2 package. Additionally, for variables that were not normally distributed, we employed both Wilcoxon and Kruskal-Wallis tests as part of our analytical approach. To calculate correlation coefficients, we used Pearson correlation. To generate and display survival curves for our subgroups, we used the Kaplan-Meier method. All of our tests were two-sided. To determine statistical significance, we used GraphPad Prism software package version 8.0 to perform analysis of variance (ANOVA) or unpaired Student's *t* tests. Statistical significance was determined by a *p*-value less than 0.05.

3. Results

3.1 Recognition of Antigen-presenting Prognostic (APP)-Related Genotyping

Based on the 23 APP genes, we obtained two genotypes through cluster analysis: APP cluster 1 and APP cluster 2 (Fig. 1A). The principal component analysis plot

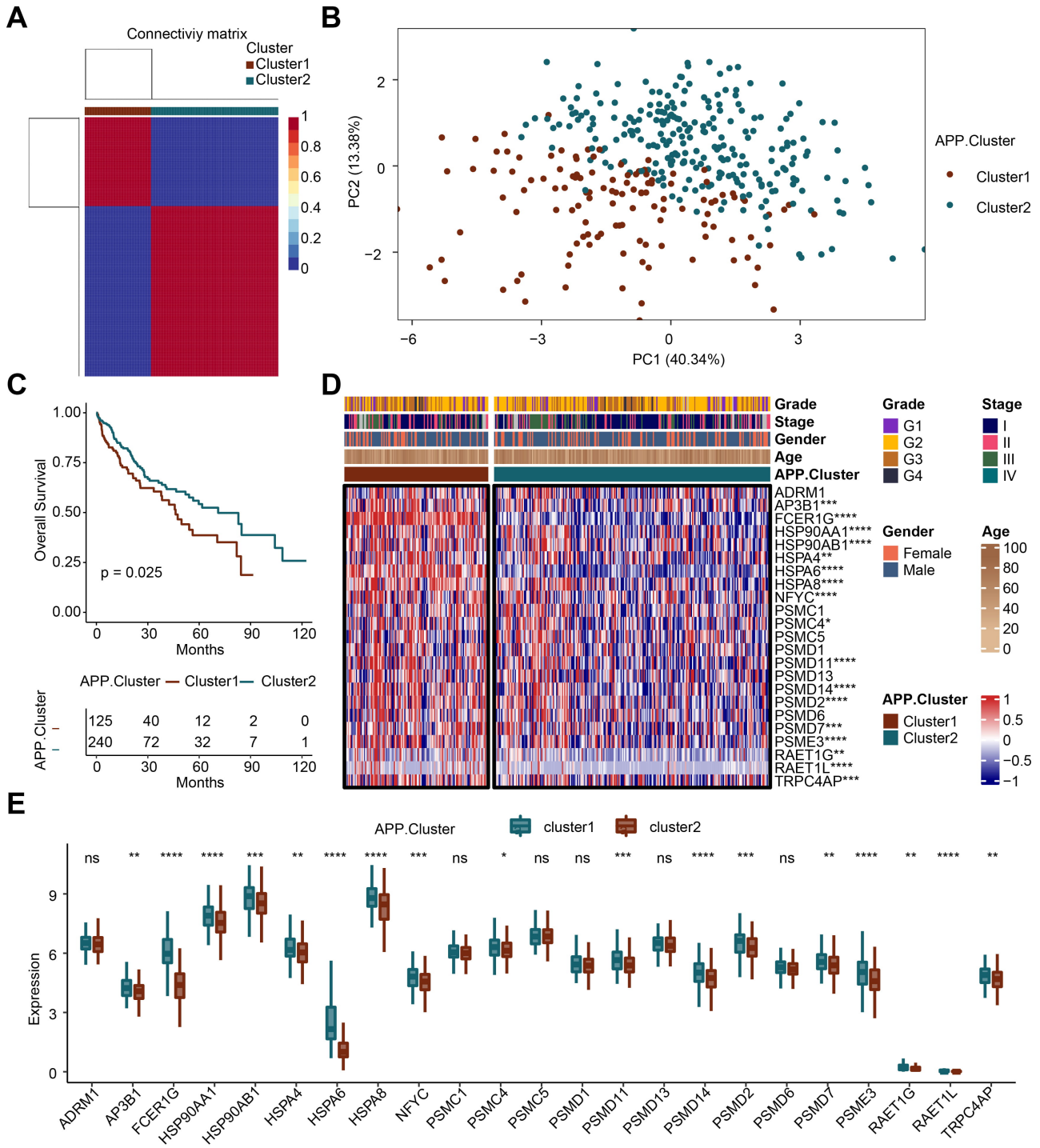

Fig. 1. Recognition of antigen-presenting prognostic (APP)-related genotyping. (A) Cluster analysis. (B) Principal component analysis (PCA) analysis. (C) Survival analysis. (D) Heatmap. (E) Bar plot. *$p < 0.05$; **$p < 0.01$; ***$p < 0.001$; ****$p < 0.0001$; ns means no statistical significance; vs. the APP. cluster 1.

showed that APP cluster 1 and APP cluster 2 had good dispersion (Fig. 1B). We conducted survival analysis on the two clusters. When the survival rate was 0.5, the survival time of cluster 2 was longer than that of cluster 1 (Fig. 1C). Subsequently, the differential expression of the 23 APP genes in cluster 1 and cluster 2 was analyzed (Fig. 1D,E). The results showed that compared with cluster 1, 17 genes including adaptor-related protein complex 3 subunit beta 1, Fc Fragment of IgE Receptor Ig (*FCER1G*), *HSP90AA1*, *HSP90AB1*, *HSPA4*, *HSPA6*, *HSPA8*, nuclear transcription factor Y subunit gamma, proteasome 26S subunit ATPase 4, proteasome 26S subunit, non-ATPase 11

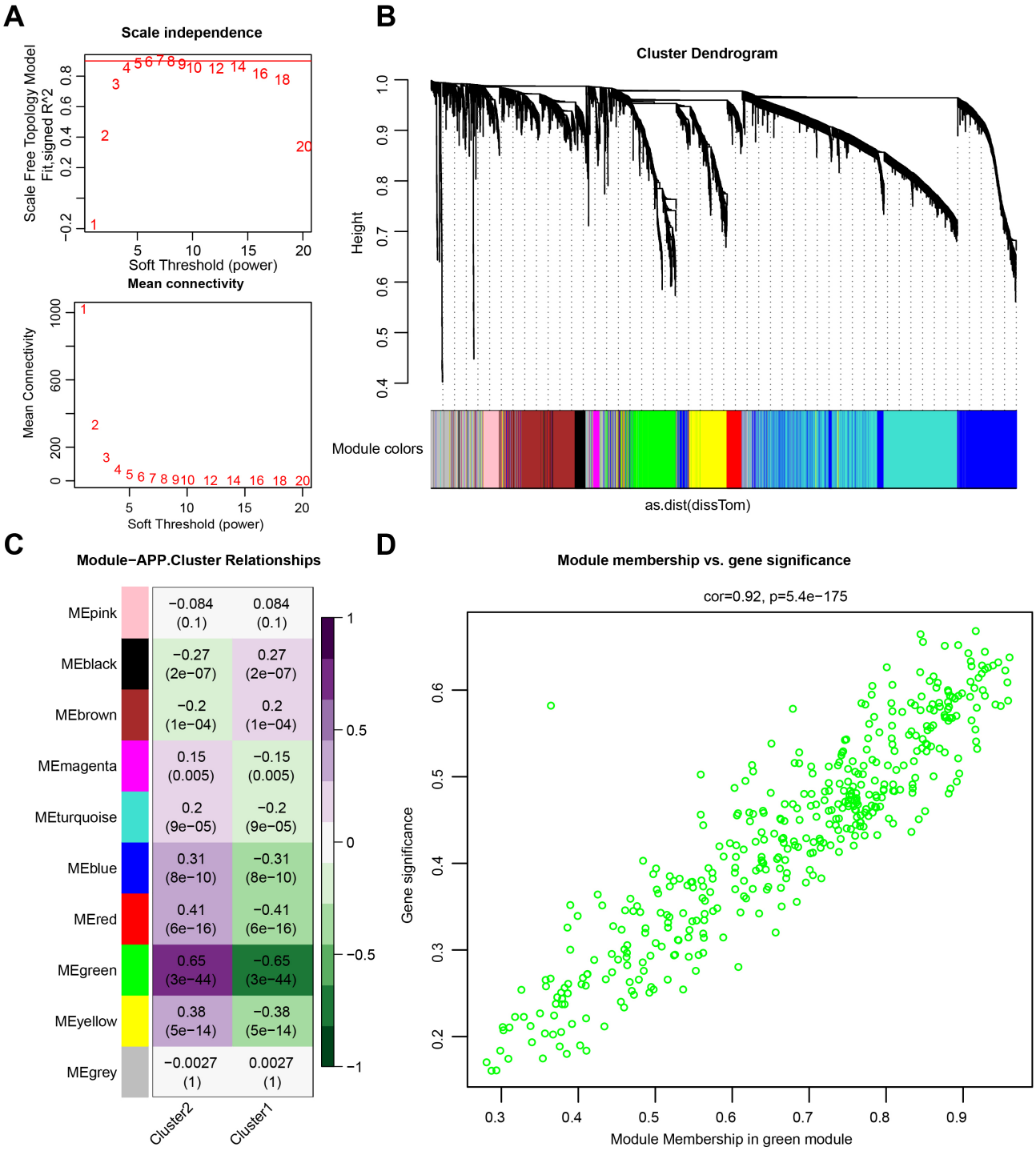

Fig. 2. Weighted gene co-expression network analysis (WGCNA). (A) Network topology analysis. (B) Module clustering tree. (C) Phenotypic and module correlation plot. (D) Correlation analysis between genes and phenotypes in modules.

(*PSMD11*), *PSMD14*, *PSMD2*, *PSMD7*, proteasome activator complex subunit 3, retinoic acid early transcript 1G (*RAET1G*), *RAET1L*, and transient receptor potential cation channel, subfamily C, member 4 associated protein were downregulated in cluster 2. The above results reveal that the APP-related genotyping analysis is reasonable.

3.2 Acquisition of Green Gene Modules Using WGCNA

The minimum soft threshold value for building a scale-free network was 5 (scale-free fit index = 0.9). Therefore, 5 was chosen as the optimal soft threshold value for subsequent analyses. Another Figure showed the network connectivity under soft thresholding power (Fig. 2A). Subsequently, a gene clustering tree was constructed (Fig. 2B).

The correlation and significance of different gene modules with cluster 1 and cluster 2 are shown in Fig. 2C. The green gene module exhibited the highest correlation with both cluster 1 and cluster 2. Further analyses revealed a positive correlation between module membership and gene significance (Fig. 2D), suggesting that genes highly related to cluster 1 and cluster 2 were also crucial in the green gene module.

3.3 Construction of APP.Score

Subsequently, 39 genes were obtained by performing univariate analysis on the genes in the green module (Fig. 3A). Nine significant genes, including *KLRB1*, *NCF2*, *PLA2G7*, *MSC*, *HSPA6*, *NPL*, *FCER1G*, *SPP1*, and *FABP5P7*, were obtained through further RF analysis (Fig. 3B). Then a LASSO model was constructed. Seven genes, including *KLRB1*, *NCF2*, P*LA2G7*, *MSC*, *HSPA6*, *SPP1*, and *FABP5P7*, were selected. Finally, the APP.Score was obtained by calculating the formula (APP.Score = –2.2047 × *KLRB1* + 0.0197 × *NCF2* + 1.2247 × *PLA2G7* + 0.7626 × *MSC* + 0.78 × *HSPA6* + 0.7743 × *SPP1* + 0.8317 × *FABP5P7*) (Fig. 3C). Upon further investigation, it was discovered that patients with a high APP.Score experienced a greater number of deaths than those with a low APP.Score (Fig. 3D). The area under the curve (AUC) values were 0.734, 0.747, and 0.679 for survival periods of 1, 2, and 3 years, respectively (Fig. 3E–G). These results suggest that APP.Score is a risk factor for HCC.

3.4 Immune Cell Infiltration and Immune Checkpoint

Supplementary Fig. 2A shows that with the increase in APP.Score, the expression of *KLRB1*, *NCF2*, *PLA2G7*, *MSC*, *HSPA6*, *SPP1*, and *FABP5P7* was significantly increased. With the increase in APP.Score, stromal score, immune score, estimate score, B cells, $CD4^+$ T cells, $CD8^+$ T cells, neutrophil, MAC, and DC enrichment were significantly increased, whereas tumor purity enrichment was significantly decreased (**Supplementary Fig. 2B**). With the increase in APP.Score, the related genes were significantly enriched including AP-related (e.g., *HLA-DRB5*, *HLA-DQB1*, and *HLA-DPB1*), cell adhesion-related (integrin subunit beta 2 and intercellular adhesion molecule 1), co-inhibitor-related (e.g., cluster of differentiation 274 [*CD274*], butyrophilin subfamily 3 member A2 [*BTN3A2*], and *BTN3A1*), co-stimulator-related (*CD80* and *CD28*), ligand-related (e.g., tumor necrosis factor [*TNF*], *TNFSF4*, *CD70*, and interferon alpha 1), receptor-related (e.g., T cell immunoreceptor with Ig and immunoreceptor tyrosine-based inhibitory motif domains, interleukin 2 receptor subunit alpha, and TNF receptor superfamily member 14), and others (e.g., indoleamine 2, 3-dioxygenase 1, granzyme A, perforin 1, high mobility group box 1 protein, and ectonucleoside triphosphate diphosphohydrolase 1), whereas *ARG1* enrichment was significantly decreased (**Supplementary Fig. 2C**).

3.5 Mutation and CNV Analyses

We further analyzed the correlation of mutated genes in the high and low APP.Score groups. In the high APP.Score group, tumor protein p53 (*TP53*) and retinoblastoma 1 (*RB1*) might have co-occurring mutations; β-catenin (*CTNNB1*) might have co-occurring mutations with WD repeat domain 87 (*WDR87*), obscurin (*OBSCN*), and mucin 16 (*MUC16*); TTN might have co-occurring mutations with low-density lipoprotein receptor-related protein 1B (*LRP1B*) and dedicator of cytokinesis protein 2 (*DOCK2*); MUC16 might have co-occurring mutations with ATP-binding cassette sub-family A member 13 (*ABCA13*); albumin (*ALB*) might have co-occurring mutations with Piccolo presynaptic cytomatrix protein (*PCLO*); ryanodine receptor 2 (*RYR2*) might have co-occurring mutations with *WDR87*, adhesion G protein-coupled receptor V1 (*ADGRV1*), and *DOCK2*; *OBSCN* might have co-occurring mutations with filaggrin (*FLG*); *PCLO* might have co-occurring mutations with *WDR87* and *ABCA13*; *ABCA13* might have co-occurring mutations with *CUB* and Sushi domain-containing protein 3; *DOCK2* might have co-occurring mutations with *FLG*; and *ADGRV1* might have co-occurring mutations with *WDR87*. In the low APP.Score group, *TP53* might have co-occurring mutations with *KMT2D*; *MUC16* might have co-occurring mutations with *RYR2*; *ALB* might have co-occurring mutations with *XIRP2*; *HMCN1* might have co-occurring mutations with *RYR2*; *LRP1B* might have co-occurring mutations with *FBN2*; and *CTNNB1* might not have co-occurring mutations with *AXIN1* and *TP53*. These results indicate that the number of gene pairs with simultaneous mutations would be greater in the high APP.Score group than in the low APP.Score group (Fig. 4A). In addition, there were differences in CNV frequency between the high and low APP.Score groups (Fig. 4B). These results indicate the significant involvement of APP.Score in both mutations and CNVs.

3.6 Prediction of Drug Sensitivity

We further analyzed the difference in drug sensitivity between the high and low APP.Score groups. In all of the drug sensitivity analyses, including temozolomide 1375, otx015 1626, leflunomide 1578, i-bet-762 1624, gdc0810 1925, dasatinib 1079, bpd-00008900 1998, bdp-00009066 1866, and azd5153 1706, the drug sensitivity of the high APP.Score group was higher than that of the low APP.Score group (Fig. 5).

3.7 In Vitro Validation of Gene Expression of APP.Score

We further analyzed the expression differences in *KLRB1*, *PLA2G7*, *MSC*, *HSPA6*, *SPP1*, and *NCF2* between the tumor and normal groups using the TCGA-LIHC dataset. Compared with the LX-2 group, the expression of *KLRB1*, *PLA2G7*, *MSC*, *HSPA6*, and *SPP1* but not *NCF2* was significantly upregulated in the HepG2 and Huh-7 groups. The difference in *KLRB1* and *PLA2G7* expres-

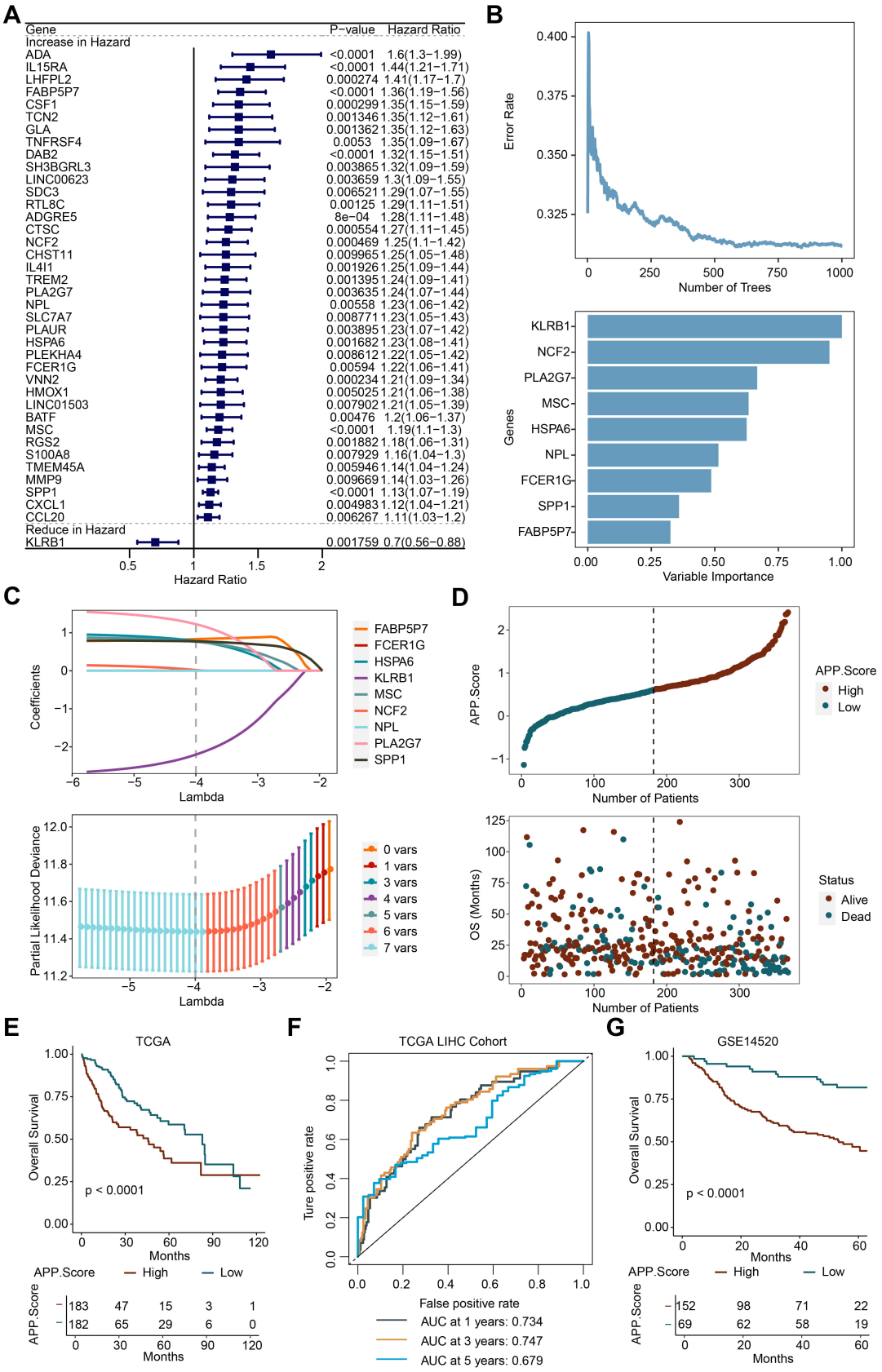

Fig. 3. APP.Score was a risk factor for Liver Hepatocellular Carcinoma (LIHC). (A) Univariate analysis. (B) Random forest (RF). (C) Lasso analysis. (D) Risk evaluation of APP.Score. (E) The Cancer Genome Atlas (TCGA) survival analysis. (F) Receiver operator characteristic (ROC) curve. (G) GSE14520 survival analysis.

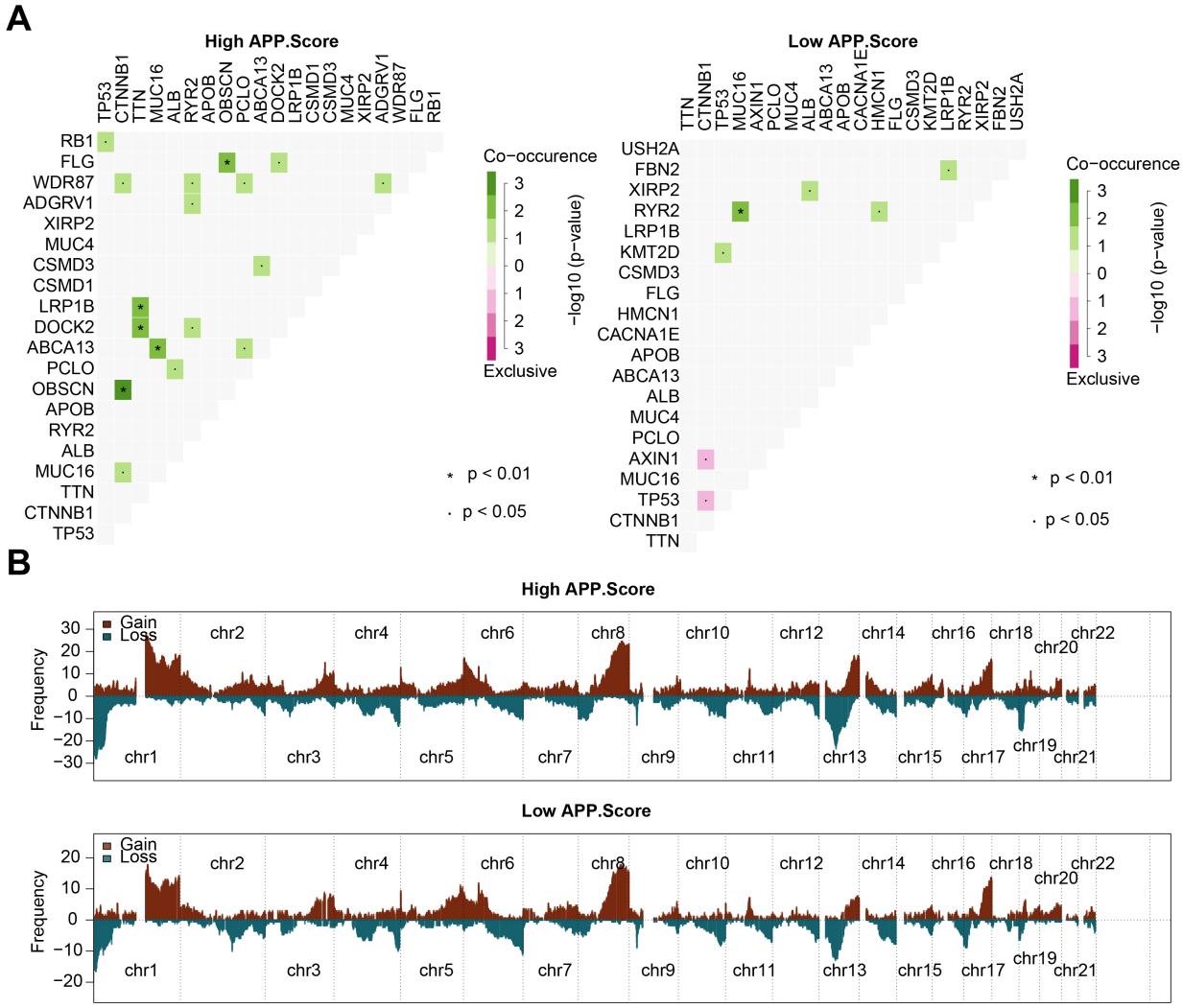

Fig. 4. Mutation and copy number variation (CNV) analysis. (A) Correlation analysis between mutated genes. (B) CNV frequency.

sion at the gene and protein levels was the most significant (Fig. 6A,B). The OS rate was 0.5, and the survival time of patients with high expression of *PLA2G7*, *MSC*, *HSPA6*, and *SPP1* was shorter, whereas that with high *KLRB1* expression was longer (Fig. 6C). Therefore, *PLA2G7* was selected for further study.

3.8 Inhibiting PLA2G7 Affects the Functions of HCC Cells HepG2 and Huh-7 Cells

Firstly, *PLA2G7* was silenced in HepG2 and Huh-7 HCC cell lines (Fig. 7A,B). Compared to the si-NC group, the cell proliferation, migration, and invasion abilities of the si-PLA2G7 group were suppressed, while the level of cell apoptosis was significantly increased (Fig. 7C–G).

3.9 PLA2G7 Affects PD-L1 Expression via STAT1

We performed GSEA for PLA2G7, which was enriched for PD-L1 expression and the PD-1 checkpoint pathway in cancer, and the PI3K/AKT, and Janus kinase/STAT pathways; si-PLA2G7 inhibited PD-L1 expression (**Supplementary Fig. 3** and Fig. 8A–C). The levels of PI3K, AKT, and p-NF-κB/NF-κB were elevated in the si-PLA2G7 group, while the level of p-STAT1/STAT1 was clearly diminished (Fig. 8D). The STAT1 activator, 2-NP, reversed the decreased PD-L1 expression caused by si-PLA2G7 (Fig. 8E), showing that PLA2G7 can affect PD-L1 expression via STAT1.

4. Discussion

Dysfunctional antigen presentation has been identified as a key factor that causes tumor progression and immune therapy resistance [31]. Antigen presentation gene disruption is one of the reasons for the loss of antigen presentation and a common event leading to immune escape in cancer [13,32]. This study focused on APPGs, and screened for core APPGs that might affect HCC. Based on this, APP.Score was calculated. APP.Score was positively associated with immune cell infiltration, expression of ICI-related genes, immune and inflammatory pathways, antigen

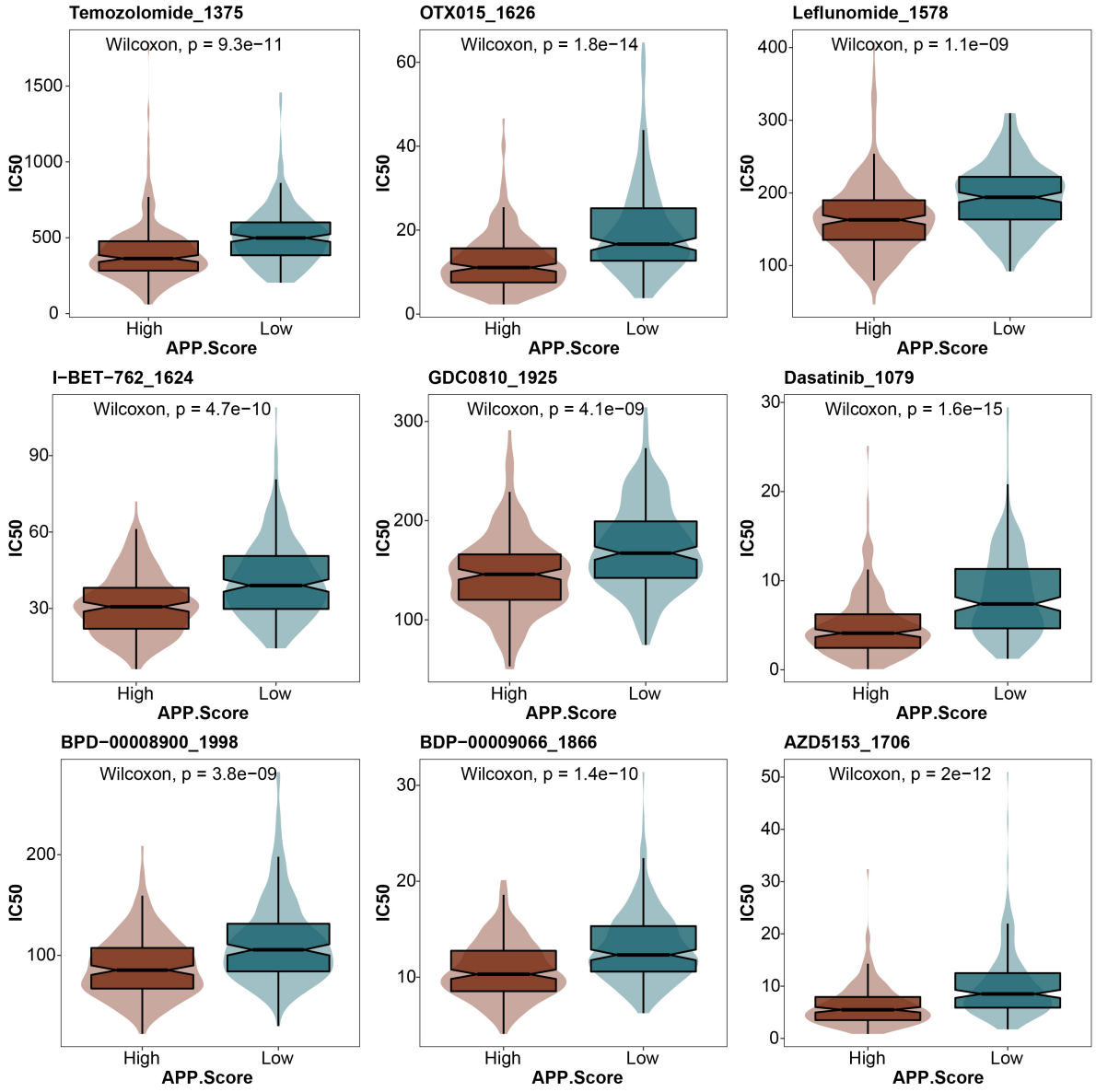

Fig. 5. Prediction of drug sensitivity.

mutations occurring simultaneously, and drug sensitivity, and was negatively correlated with OS. The AUC values were 0.734, 0.747, and 0.679 for survival periods of 1, 2, and 3 years, respectively, indicating that APP.Score may serve as an independent prognostic factor for patients with HCC. *SPP1* was obviously overexpressed in HCC in the TCGA-LIHC dataset. With the exception of KLRB1, the high expression group of the five core APPGs (*PLA2G7*, *MSC*, *HSPA6*, *SPP1*, and *NCF2*) had lower survival rates than the low expression group. Furthermore, *in vitro* experiments showed that the significant expression of the five core APPGs (*KLRB1*, *PLA2G7*, *MSC*, *HSPA6*, and *SPP1*) was increased in HCC cell lines, and *PLA2G7* silencing inhibited the development of cancer cells.

In recent years, several studies have used methods such as WGCNA, RF, and LASSO to reveal the related risk factors and potential mechanisms of immune escape in different tumors [33,34]. For example, Zhong *et al.* [33] mainly used WGCNA to reveal that syndecan-1 may be related to immune infiltration and regulate AP. Chen *et al.* [34] mainly used WGCNA and LASSO methods to find that the high-risk group (based on the hypoxia-related gene risk model) displayed a unique immune-suppressive microenvironment, lower levels of AP, and higher levels of suppressive cytokines. However, the screening of core APPGs and its potential immune function prediction in HCC have been poorly reported. The current study found that seven core APPGs (*KLRB1*, *PLA2G7*, *MSC*, *HSPA6*, *SPP1*, *NCF2*, and *FABP5P7*) and APP.Score were obtained through NMF clustering, WGCNA, RF, and LASSO methods in HCC.

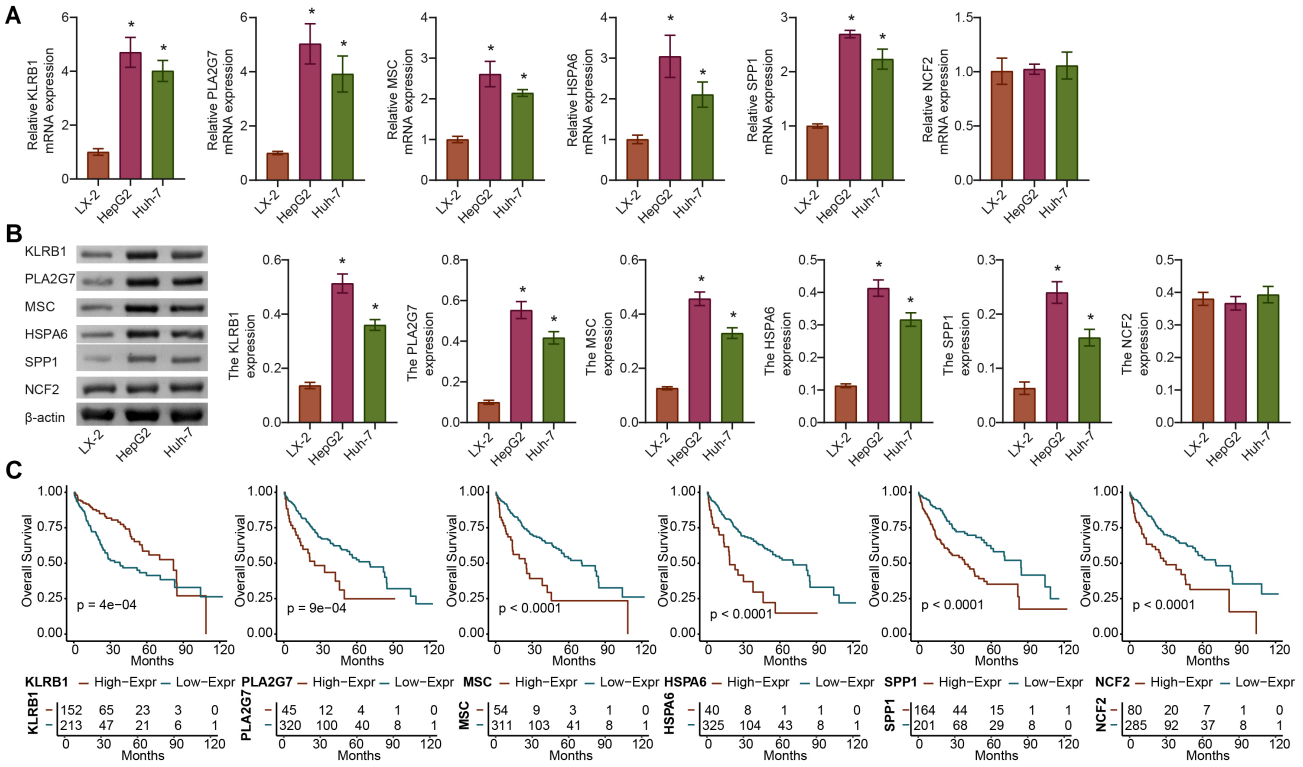

Fig. 6. *In vitro* validation of gene expression of APP.Score. (A,B) The expression of genes (*KLRB1*, *PLA2G7*, *MSC*, *HSPA6*, *SPP1*, and *NCF2*) of APP.Score. (C) Survival curves of the six genes (*KLRB1*, *PLA2G7*, *MSC*, *HSPA6*, *SPP1*, and *NCF2*) used to construct the APP.Score were analyzed. Analysis of variance (ANOVA). *$p < 0.05$, vs. LX-2.

KLRB1, encoded by the killer cell lectin-like receptor B1 gene, is a newly reported candidate inhibitor of tumor-infiltrating T cells [35]. KLRB1 is a potential a potential new immune checkpoint, and may synergize with other ICIs to regulate the immune microenvironment, thus it can be used to develop new immunotherapeutically targeted drugs [36]. $CD8^+$ T cells overexpressing KLRB1 are in a state of low innate cytotoxicity in recurrent HCC [37]. MSC (also known as activated B-cell factor 1, ABF-1) inhibits plasma cell differentiation but promotes memory B-cell formation [38]. *HSPA6* is an antigen processing and presentation gene. When HSPA6 is released into the extracellular space, it serves as a source of antigen as it enables peptide conjugation and induces cross-presentation of antigen from DCs to T cells [39]. In cervical cancer, the expression level of HSPA6 is negatively correlated with survival [40]. High levels of HSPA6 may be associated with the early recurrence of HCC [41]. Similarly, our study found that the expression of *HSPA6* (one of the core APPGs) was significantly elevated and negatively correlated with survival. Liu *et al.* [42] found that SPP1 is an immune-related predictive factor for low survival rates in HCC patients. SPP1 upregulates PD-L1-mediated macrophage polarization and promotes immune escape from lung adenocarcinoma [43]. NCF2 is a subunit of a multiprotein complex known as nicotinamide adenine dinucleotide phosphate (NADPH) oxidase, which has been shown to regulate antigen processing and MHC-I cross-presentation in dendritic cells. Thus *NCF2* has been shown to be an APPGs [44]. PLA2G7 is a protein produced by macrophages. Reduction of PLA2G7 may mediate the immunometabolic effects of caloric restriction and be used to reduce inflammation and extend healthy lifespan [45,46]. Bioinformatics analysis and experiments confirmed that PLA2G7 can serve as a potential immune-related biomarker and contribute to chronic obstructive pulmonary disease progression by promoting the expansion and inhibitory function of myeloid-derived suppressor cells [47]. *PLA2G7* has also been found to be strongly associated with TME composition, so that patients with diffuse large B-cell lymphoma expressing higher levels of this gene exhibit higher levels of localized monocytes and gamma delta T cells [48]. PLA2G7 is highly expressed in subgroups of metastatic and invasive breast cancer and metastatic samples from various origin tissues, promoting the development of cultured breast cancer cells [49]. However, the occurrence of core APPGs, such as *KLRB1*, *PLA2G7*, *MSC*, *HSPA6*, and *SPP1*, in HCC is rarely documented. In short, the current research showed the significant upregulation of five core APPGs (*KLRB1*, *PLA2G7*, *MSC*, *HSPA6*, and *SPP1*) in HCC cell lines, and *PLA2G7* silencing inhibited cancer cell growth and promoted cells apoptosis. In addition, our study identified *PLA2G7*, a

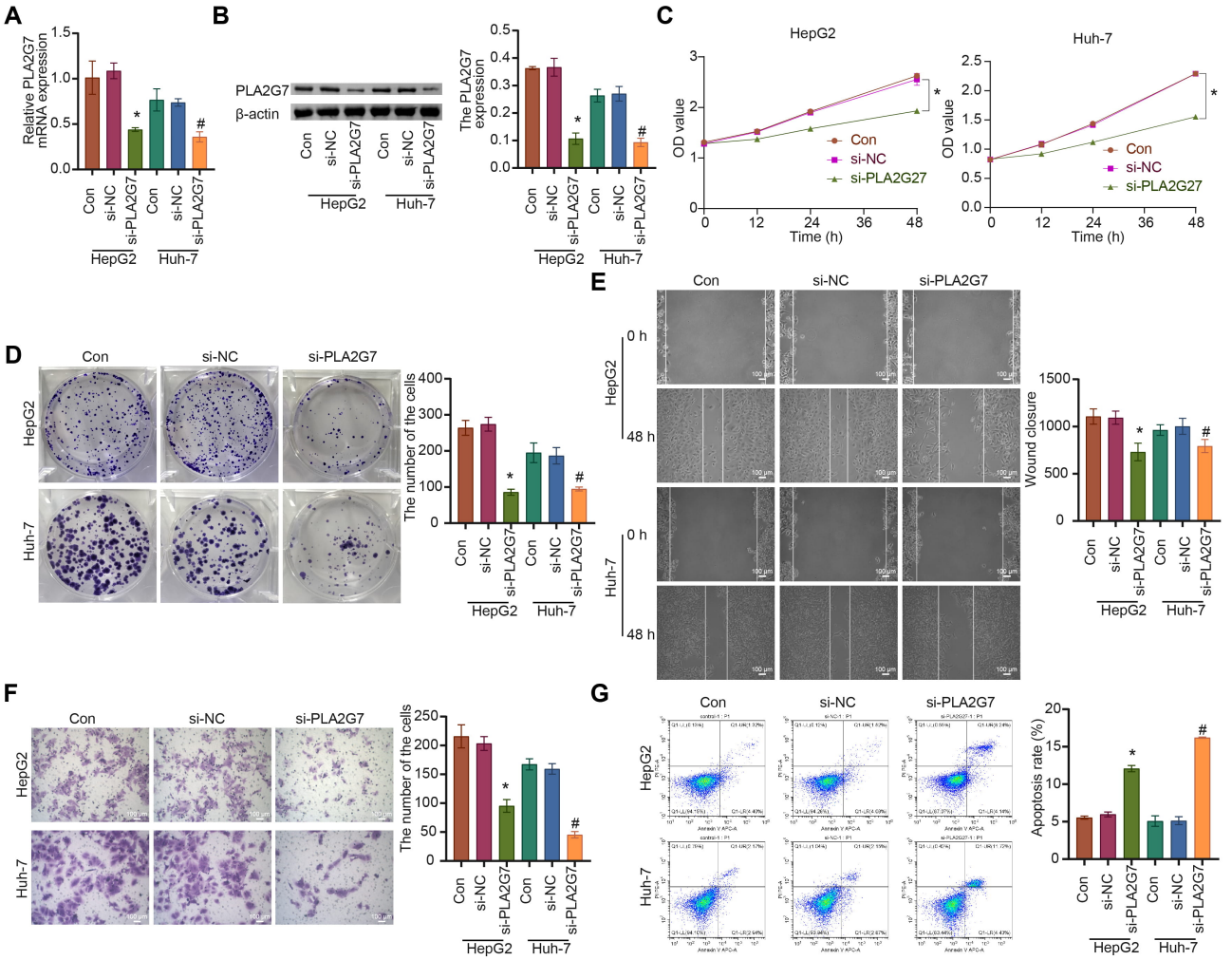

Fig. 7. Inhibiting *PLA2G7* affects the functions of hepatocellular carcinoma (HCC) cells HepG2 and Huh-7. (A,B) The expression of *PLA2G7* was detected. (C) The cell proliferation (0, 12, 24, 48 h) was measured. (D) The cell proliferation ability was analyzed. (E) The cell migration was measured. (F) The cell invasion was analyzed. (G) The cell apoptosis level was assessed. ANOVA. *$p < 0.05$, vs. the si-PLA2G7 group (HepG2); #$p < 0.05$, vs. the si-PLA2G7 group (Huh-7).

novel regulator of PD-L1, as a potential target for cancer therapy. PD-L1 may increase the inflammatory response in the TME and promote neoantigen presentation, as well as anti-tumor immune escape [50]. Therefore, we hypothesize that PLA2G7 may regulate antigen presentation through PD-L1. However, this needs to be further investigated in the future.

It is well known that common APCs include DCs, MACs, and B cells [51]. Dysregulation of APCs is an important cause of tumor immune escape [14]. In cancer, APCs present peptides on their HLA to naïve T cells ($CD8^+$ or $CD4^+$) to activate an immune response [11,12]. APCs are associated with many genes related to immune function, such as *CD80*, *CD274* (encoded PD-L1), and *CD276* [52,53]. This study found that APP.Score was positively correlated with immune cell infiltration (e.g., $CD8^+$ T cells, DCs, and MACs), expression of ICI-related genes (e.g., APCs, receptor, co-inhibitor, and cell adhesion molecules), and immune and inflammatory-related pathways (e.g., PD-L1 expression and PD-1 checkpoint, antigen processing and presentation, and p53 pathways). It is known that the successful completion of antigen-presenting machinery (APM), i.e., tumor antigens are correctly recognized and processed, and then presented to immune effector cells such as $CD8^+$ cytotoxic T-cells, which is a key prerequisite for the efficacy of immunotherapy [54]. However, the mechanism between APPGs and immune evasion in HCC is still not fully investigated, which is a limitation of our study.

Mutations or heterozygous loss of MHC-I can also cause damage to the antigen presentation system [55]. Cai *et al.* [56] found that the most common mutated genes predicting MHC-II neoantigens in lung adenocarcinoma patients included TTN, RYR2, MUC16, and TP53. In breast cancer, TP53 mutation is linked to both a poor prognosis and immune cell infiltration [57]. Long *et al.* [58] found that TP53 mutation is commonly associated with HCC and

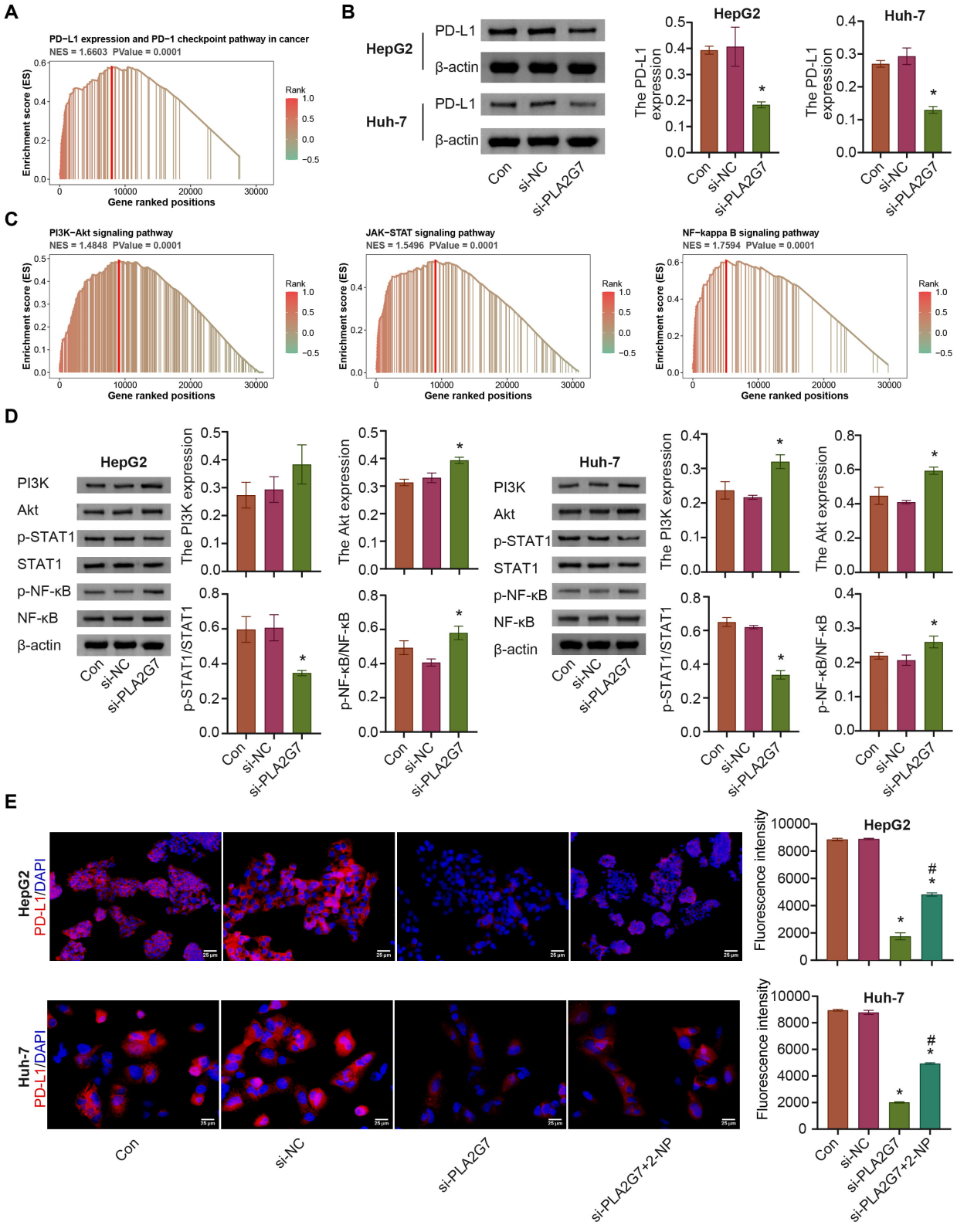

Fig. 8. PLA2G7 affects PD-L1 expression via STAT1. (A) PLA2G7 was enriched in the PD-L1 pathway. (B) The expression of PD-L1 was detected. (C) PLA2G7 was enriched in the PI3K-Akt, JAK-STAT, and nuclear factor kappa B (NF-κB) pathway. (D) The expression of PI3K, Akt, phosphorylated signal transducer and activator of transcription 1 (p-STAT1), STAT1, p-NF-κB, and NF-κB was measured. (E) The cells were treated with STAT1 activator (2-NP, 45 µmol/L) for 1 h. The fluorescence intensity of PD-L1 was observed. ANOVA. *$p < 0.05$, vs. the si-NC group; #$p < 0.05$, vs. the si-PLA2G7 group.

negatively impacts its progression and outcome. It also impairs the immune response of patients with HCC. Wang *et al*. [59] reported that these are the most frequently mutated genes in Chinese patients with HCC include TP53, RB1, CCND1, and AT-rich interactive domain-containing protein 1A. Among these mutated genes, TTN mutation is usually associated with poor immune infiltration and a worse HCC prognosis [60]. Our study found that a high APP.Score might be associated with more gene pairs with a concurrent mutation in tumor antigens (e.g., TP53 and RB1), suggesting that APP.Score might be related to poor prognosis. Zhou *et al*. [61] reported that MHC-I antigen-presenting enhanced cancer immunotherapy. Enhanced tumor antigen-presenting contributes to synergistic anti-PD-1 therapy for metastatic breast cancer [62]. Our study discovered a positive correlation between APP.Score and expression of ICI-related genes, a positive correlation between APP.Score and drug sensitivity, and a negative correlation between the APP.Score and survival. ROC curve analysis showed the AUC values were 0.734, 0.747, and 0.679 for survival periods of 1, 2, and 3 years, respectively, indicating that the APP.Score may serve as an independent prognostic factor for patients with HCC. In conclusion, APP.Score may help to facilitate the clinical management of HCC.

Activation of STAT1 promotes PD-L1 expression, enhancing the effect of PD-L1 blockade in a mouse model of lung cancer [63]. STAT1 can bind to the PD-L1 promoter and thus transcriptionally regulate PD-L1 expression [64]. In HCC, activation of STAT1 promotes PD-L1 expression [65]. Our results suggest that si-PLA2G7 may inhibit PD-L1 expression by repressing the STAT1 pathway. Our study identified PLA2G7, a novel regulator of PD-L1, as a potential target for cancer therapy. PLA2G7 may be a novel target for ICI therapy.

Due to the complexity and difficulty of collecting clinical specimens, the expression of the core APPGs in HCC tissue has not been further validated. We did not explore the effects of PLA2G7 on immune cells for the study, which is a limitation of our study. In addition, considering that *FABP5P7* is a mostly non-coding pseudo genes [66], we have not yet studied its expression and functional effects in HCC. We plan to study this further in the future.

5. Conclusions

In this study, a risk scoring model, APP.Score, was successfully constructed based on seven core APPGs in LIHC, namely, *KLRB1*, *PLA2G7*, *MSC*, *HSPA6*, *SPP1*, *NCF2*, and *FABP5P7*. *In vitro* experiments showed the significant upregulation of five core APPGs (*KLRB1*, *PLA2G7*, *MSC*, *HSPA6*, and *SPP1*) in HCC cell lines, and inhibition of PLA2G7 significantly suppressed cancer cell development and PD-L1 expression. The study provides a new perspective and potential target for immune research on antigen presentation in HCC.

Availability of Data and Materials

All data found in this study are included in the manuscript or are available upon request by contact with the first author or corresponding author.

Author Contributions

QY designed the research study. SG performed the research, and analyzed the data. SG wrote the manuscript. Both authors contributed to editorial changes in the manuscript. Both authors read and approved the final manuscript. Both authors have participated sufficiently in the work and agreed to be accountable for all aspects of the work.

Ethics Approval and Consent to Participate

Not applicable.

Acknowledgment

Not applicable.

Funding

This research received no external funding.

Conflict of Interest

The authors declare no conflict of interest.

Supplementary Material

Supplementary material associated with this article can be found, in the online version, at https://doi.org/10.31083/j.fbl2901039.

References

[1] Anwanwan D, Singh SK, Singh S, Saikam V, Singh R. Challenges in liver cancer and possible treatment approaches. Biochimica et Biophysica Acta. Reviews on Cancer. 2020; 1873: 188314.

[2] Li X, Ramadori P, Pfister D, Seehawer M, Zender L, Heikenwalder M. The immunological and metabolic landscape in primary and metastatic liver cancer. Nature Reviews. Cancer. 2021; 21: 541–557.

[3] Choi DT, Davila JA, Sansgiry S, David E, Singh H, El-Serag HB, *et al*. Factors Associated With Delay of Diagnosis of Hepatocellular Carcinoma in Patients With Cirrhosis. Clinical Gastroenterology and Hepatology: the Official Clinical Practice Journal of the American Gastroenterological Association. 2021; 19: 1679–1687.

[4] Zhou Q, Lin J, Yan Y, Meng S, Liao H, Chen R, *et al*. INPP5F translocates into cytoplasm and interacts with ASPH to promote tumor growth in hepatocellular carcinoma. Journal of Experimental & Clinical Cancer Research: CR. 2022; 41: 13.

[5] Xu F, Jin T, Zhu Y, Dai C. Immune checkpoint therapy in liver cancer. Journal of Experimental & Clinical Cancer Research: CR. 2018; 37: 110.

[6] Llovet JM, Castet F, Heikenwalder M, Maini MK, Mazzaferro V, Pinato DJ, *et al*. Immunotherapies for hepatocellular carcinoma. Nature Reviews. Clinical Oncology. 2022; 19: 151–172.

[7] Tang B, Zhu J, Zhao Z, Lu C, Liu S, Fang S, *et al*. Diagnosis and prognosis models for hepatocellular carcinoma patient's man-

agement based on tumor mutation burden. Journal of Advanced Research. 2021; 33: 153–165.

[8] Lv T, Xiong X, Yan W, Liu M, Xu H, He Q. Targeting of GSDMD sensitizes HCC to anti-PD-1 by activating cGAS pathway and downregulating PD-L1 expression. Journal for Immunotherapy of Cancer. 2022; 10: e004763.

[9] Yu J, Green MD, Li S, Sun Y, Journey SN, Choi JE, *et al*. Liver metastasis restrains immunotherapy efficacy via macrophage-mediated T cell elimination. Nature Medicine. 2021; 27: 152–164.

[10] Pishesha N, Harmand TJ, Ploegh HL. A guide to antigen processing and presentation. Nature Reviews. Immunology. 2022; 22: 751–764.

[11] Kawasaki T, Ikegawa M, Kawai T. Antigen Presentation in the Lung. Frontiers in Immunology. 2022; 13: 860915.

[12] Andreani M, Gaspari S, Locatelli F. Human leucocyte antigen diversity: A biological gift to escape infections, no longer a barrier for haploidentical Hemopoietic Stem Cell Transplantation. International Journal of Immunogenetics. 2020; 47: 34–40.

[13] Dhatchinamoorthy K, Colbert JD, Rock KL. Cancer Immune Evasion Through Loss of MHC Class I Antigen Presentation. Frontiers in Immunology. 2021; 12: 636568.

[14] Jhunjhunwala S, Hammer C, Delamarre L. Antigen presentation in cancer: insights into tumour immunogenicity and immune evasion. Nature Reviews. Cancer. 2021; 21: 298–312.

[15] Lei T, Qian H, Lei P, Hu Y. Ferroptosis-related gene signature associates with immunity and predicts prognosis accurately in patients with osteosarcoma. Cancer Science. 2021; 112: 4785–4798.

[16] Gao Y, Wang H, Chen S, An R, Chu Y, Li G, *et al*. Single-cell N^6-methyladenosine regulator patterns guide intercellular communication of tumor microenvironment that contribute to colorectal cancer progression and immunotherapy. Journal of Translational Medicine. 2022; 20: 197.

[17] Tian Z, He W, Tang J, Liao X, Yang Q, Wu Y, *et al*. Identification of Important Modules and Biomarkers in Breast Cancer Based on WGCNA. OncoTargets and Therapy. 2020; 13: 6805–6817.

[18] Chen C, Hou J, Tanner JJ, Cheng J. Bioinformatics Methods for Mass Spectrometry-Based Proteomics Data Analysis. International Journal of Molecular Sciences. 2020; 21: 2873.

[19] Yu N, Wu MJ, Liu JX, Zheng CH, Xu Y. Correntropy-Based Hypergraph Regularized NMF for Clustering and Feature Selection on Multi-Cancer Integrated Data. IEEE Transactions on Cybernetics. 2021; 51: 3952–3963.

[20] Toth R, Schiffmann H, Hube-Magg C, Büscheck F, Höflmayer D, Weidemann S, *et al*. Random forest-based modelling to detect biomarkers for prostate cancer progression. Clinical Epigenetics. 2019; 11: 148.

[21] Ning S, Li H, Qiao K, Wang Q, Shen M, Kang Y, *et al*. Identification of long-term survival-associated gene in breast cancer. Aging. 2020; 12: 20332–20349.

[22] Huang X, Chen X, Chen X, Wang W. Screening of Serum miRNAs as Diagnostic Biomarkers for Lung Cancer Using the Minimal-Redundancy-Maximal-Relevance Algorithm and Random Forest Classifier Based on a Public Database. Public Health Genomics. 2022; 1–9.

[23] Kang J, Choi YJ, Kim IK, Lee HS, Kim H, Baik SH, *et al*. LASSO-Based Machine Learning Algorithm for Prediction of Lymph Node Metastasis in T1 Colorectal Cancer. Cancer Research and Treatment. 2021; 53: 773–783.

[24] Zhang C, Zheng JH, Lin ZH, Lv HY, Ye ZM, Chen YP, *et al*. Profiles of immune cell infiltration and immune-related genes in the tumor microenvironment of osteosarcoma. Aging. 2020; 12: 3486–3501.

[25] Liu XS, Zhou LM, Yuan LL, Gao Y, Kui XY, Liu XY, *et al*. NPM1 Is a Prognostic Biomarker Involved in Immune Infiltration of Lung Adenocarcinoma and Associated With m6A Modification and Glycolysis. Frontiers in Immunology. 2021; 12: 724741.

[26] Li G, Wu F, Zeng F, Zhai Y, Feng Y, Chang Y, *et al*. A novel DNA repair-related nomogram predicts survival in low-grade gliomas. CNS Neuroscience & Therapeutics. 2021; 27: 186–195.

[27] Zhang L, Zhang X, Guan M, Yu F, Lai F. In-depth single-cell and bulk-RNA sequencing developed a NETosis-related gene signature affects non-small-cell lung cancer prognosis and tumor microenvironment: results from over 3,000 patients. Frontiers in Oncology. 2023; 13: 1282335.

[28] Li S, Zhang N, Liu S, Zhang H, Liu J, Qi Y, *et al*. ITGA5 Is a Novel Oncogenic Biomarker and Correlates With Tumor Immune Microenvironment in Gliomas. Frontiers in Oncology. 2022; 12: 844144.

[29] Maeser D, Gruener RF, Huang RS. oncoPredict: an R package for predicting in vivo or cancer patient drug response and biomarkers from cell line screening data. Briefings in Bioinformatics. 2021; 22: bbab260.

[30] Wang S, Chen X, Cheng J, Cai T, Wu X, Cheng Z, *et al*. Calunduloside E inhibits HepG2 cell proliferation and migration via p38/JNK-HMGB1 signalling axis. Journal of Pharmacological Sciences. 2021; 147: 18–26.

[31] Zhou L, Mudianto T, Ma X, Riley R, Uppaluri R. Targeting EZH2 Enhances Antigen Presentation, Antitumor Immunity, and Circumvents Anti-PD-1 Resistance in Head and Neck Cancer. Clinical Cancer Research: an Official Journal of the American Association for Cancer Research. 2020; 26: 290–300.

[32] Kotsias F, Cebrian I, Alloatti A. Antigen processing and presentation. International Review of Cell and Molecular Biology. 2019; 348: 69–121.

[33] Zhong J, Shi S, Peng W, Liu B, Yang B, Niu W, *et al*. Weighted Gene Co-Expression Network Analysis (WGCNA) Reveals the Functions of Syndecan-1 to Regulate Immune Infiltration by Influenced T Cells in Glioma. Frontiers in Genetics. 2022; 13: 792443.

[34] Chen X, Lan H, He D, Xu R, Zhang Y, Cheng Y, *et al*. Multi-Omics Profiling Identifies Risk Hypoxia-Related Signatures for Ovarian Cancer Prognosis. Frontiers in Immunology. 2021; 12: 645839.

[35] Konduri V, Oyewole-Said D, Vazquez-Perez J, Weldon SA, Halpert MM, Levitt JM, *et al*. $CD8^+CD161^+$ T-Cells: Cytotoxic Memory Cells With High Therapeutic Potential. Frontiers in Immunology. 2021; 11: 613204.

[36] Zhou X, Du J, Liu C, Zeng H, Chen Y, Liu L, *et al*. A Pan-Cancer Analysis of CD161, a Potential New Immune Checkpoint. Frontiers in Immunology. 2021; 12: 688215.

[37] Sun Y, Wu L, Zhong Y, Zhou K, Hou Y, Wang Z, *et al*. Single-cell landscape of the ecosystem in early-relapse hepatocellular carcinoma. Cell. 2021; 184: 404–421.e16.

[38] Chiu YK, Lin IY, Su ST, Wang KH, Yang SY, Tsai DY, *et al*. Transcription factor ABF-1 suppresses plasma cell differentiation but facilitates memory B cell formation. Journal of Immunology (Baltimore, Md.: 1950). 2014; 193: 2207–2217.

[39] Milani V, Noessner E, Ghose S, Kuppner M, Ahrens B, Scharner A, *et al*. Heat shock protein 70: role in antigen presentation and immune stimulation. International Journal of Hyperthermia: the Official Journal of European Society for Hyperthermic Oncology, North American Hyperthermia Group. 2002; 18: 563–575.

[40] Qin K, Jian D, Xue Y, Cheng Y, Zhang P, Wei Y, *et al*. DDX41 regulates the expression and alternative splicing of genes involved in tumorigenesis and immune response. Oncology Reports. 2021; 45: 1213–1225.

[41] Yang Z, Zhuang L, Szatmary P, Wen L, Sun H, Lu Y, *et al*. Upregulation of heat shock proteins (HSPA12A, HSP90B1, HSPA4, HSPA5 and HSPA6) in tumour tissues is associated with

poor outcomes from HBV-related early-stage hepatocellular carcinoma. International Journal of Medical Sciences. 2015; 12: 256–263.

[42] Liu L, Zhang R, Deng J, Dai X, Zhu X, Fu Q, *et al*. Construction of TME and Identification of crosstalk between malignant cells and macrophages by SPP1 in hepatocellular carcinoma. Cancer Immunology, Immunotherapy: CII. 2022; 71: 121–136.

[43] Zhang Y, Du W, Chen Z, Xiang C. Upregulation of PD-L1 by SPP1 mediates macrophage polarization and facilitates immune escape in lung adenocarcinoma. Experimental Cell Research. 2017; 359: 449–457.

[44] Yang S, Tang D, Zhao YC, Liu H, Luo S, Stinchcombe TE, *et al*. Potentially functional variants of ERAP1, PSMF1 and NCF2 in the MHC-I-related pathway predict non-small cell lung cancer survival. Cancer Immunology, Immunotherapy. 2021; 70: 2819–2833.

[45] Spadaro O, Youm Y, Shchukina I, Ryu S, Sidorov S, Ravussin A, *et al*. Caloric restriction in humans reveals immunometabolic regulators of health span. Science (New York, N.Y.). 2022; 375: 671–677.

[46] Rhoads TW, Anderson RM. Caloric restriction has a new player. Science (New York, N.Y.). 2022; 375: 620–621.

[47] Zhao X, Yue Y, Wang X, Zhang Q. Bioinformatics analysis of PLA2G7 as an immune-related biomarker in COPD by promoting expansion and suppressive functions of MDSCs. International Immunopharmacology. 2023; 120: 110399.

[48] Zheng W, Lin Q, Issah MA, Liao Z, Shen J. Identification of PLA2G7 as a novel biomarker of diffuse large B cell lymphoma. BMC Cancer. 2021; 21: 927.

[49] Lehtinen L, Vainio P, Wikman H, Huhtala H, Mueller V, Kallioniemi A, *et al*. *PLA2G7* associates with hormone receptor negativity in clinical breast cancer samples and regulates epithelial-mesenchymal transition in cultured breast cancer cells. The Journal of Pathology. Clinical Research. 2017; 3: 123–138.

[50] Gao Y, Nihira NT, Bu X, Chu C, Zhang J, Kolodziejczyk A, *et al*. Acetylation-dependent regulation of PD-L1 nuclear translocation dictates the efficacy of anti-PD-1 immunotherapy. Nature Cell Biology. 2020; 22: 1064–1075.

[51] Shanmugam G, Das S, Paul S, Rakshit S, Sarkar K. Clinical relevance and therapeutic aspects of professional antigen-presenting cells in lung cancer. Medical Oncology (Northwood, London, England). 2022; 39: 237.

[52] Giannoudis A, Varešlija D, Sharma V, Zakaria R, Platt-Higgins A, Rudland PS, *et al*. Characterisation of the immune microenvironment of primary breast cancer and brain metastasis reveals depleted T-cell response associated to ARG2 expression. ESMO Open. 2022; 7: 100636.

[53] Lorenzetti R, Janowska I, Smulski CR, Frede N, Henneberger N, Walter L, *et al*. Abatacept modulates CD80 and CD86 expression and memory formation in human B-cells. Journal of Autoimmunity. 2019; 101: 145–152.

[54] Yang K, Halima A, Chan TA. Antigen presentation in cancer - mechanisms and clinical implications for immunotherapy. Nature Reviews. Clinical Oncology. 2023; 20: 604–623.

[55] Yamamoto K, Venida A, Yano J, Biancur DE, Kakiuchi M, Gupta S, *et al*. Autophagy promotes immune evasion of pancreatic cancer by degrading MHC-I. Nature. 2020; 581: 100–105.

[56] Cai W, Zhou D, Wu W, Tan WL, Wang J, Zhou C, *et al*. MHC class II restricted neoantigen peptides predicted by clonal mutation analysis in lung adenocarcinoma patients: implications on prognostic immunological biomarker and vaccine design. BMC Genomics. 2018; 19: 582.

[57] Zhang Z, Hao R, Guo Q, Zhang S, Wang X. TP53 Mutation Infers a Poor Prognosis and Is Correlated to Immunocytes Infiltration in Breast Cancer. Frontiers in Cell and Developmental Biology. 2021; 9: 759154.

[58] Long J, Wang A, Bai Y, Lin J, Yang X, Wang D, *et al*. Development and validation of a TP53-associated immune prognostic model for hepatocellular carcinoma. EBioMedicine. 2019; 42: 363–374.

[59] Wang S, Shi H, Liu T, Li M, Zhou S, Qiu X, *et al*. Mutation profile and its correlation with clinicopathology in Chinese hepatocellular carcinoma patients. Hepatobiliary Surgery and Nutrition. 2021; 10: 172–179.

[60] Wang R, Hu X, Liu X, Bai L, Gu J, Li Q. Construction of liver hepatocellular carcinoma-specific lncRNA-miRNA-mRNA network based on bioinformatics analysis. PloS one. 2021; 16: e0249881.

[61] Zhou Y, Bastian IN, Long MD, Dow M, Li W, Liu T, *et al*. Activation of NF-κB and p300/CBP potentiates cancer chemoimmunotherapy through induction of MHC-I antigen presentation. Proceedings of the National Academy of Sciences of the United States of America. 2021; 118: e2025840118.

[62] Shen M, Smith HA, Wei Y, Jiang YZ, Zhao S, Wang N, *et al*. Pharmacological disruption of the MTDH-SND1 complex enhances tumor antigen presentation and synergizes with anti-PD-1 therapy in metastatic breast cancer. Nature Cancer. 2022; 3: 60–74.

[63] Taniguchi H, Caeser R, Chavan SS, Zhan YA, Chow A, Manoj P, *et al*. WEE1 inhibition enhances the antitumor immune response to PD-L1 blockade by the concomitant activation of STING and STAT1 pathways in SCLC. Cell Reports. 2022; 39: 110814.

[64] Zhang H, Zhu C, He Z, Chen S, Li L, Sun C. LncRNA PSMB8-AS1 contributes to pancreatic cancer progression via modulating miR-382-3p/STAT1/PD-L1 axis. Journal of Experimental & Clinical Cancer Research: CR. 2020; 39: 179.

[65] Peng Q, Li S, Shi X, Guo Y, Hao L, Zhang Z, *et al*. Dihydroartemisinin broke the tumor immunosuppressive microenvironment by inhibiting YAP1 expression to enhance anti-PD-1 efficacy. Phytotherapy Research: PTR. 2023; 37: 1740–1753.

[66] Cheetham SW, Faulkner GJ, Dinger ME. Overcoming challenges and dogmas to understand the functions of pseudogenes. Nature Reviews. Genetics. 2020; 21: 191–201.